Tone noise reduction by plasma actuator on a flat plate with blunt trailing edge

Al-Sadawi Laith[1] and Tze Pei Chong[2]
[1-2] Brunel University London, Uxbridge, UB8 3PH, UK

An experimental study of active control of vortex shedding narrow band tonal noise from both blunt and rounded trailing edge of a profiled body at zero incidences was performed using Single Dielectric Barrier plasma actuators (DBD). Acoustics and flow measurements were carried out in an open jet, aerocoustic wind tunnel at Reynolds numbers ranging from $7x10^4$ to $4x10^5$. The noise results were obtained using single microphone, while both PIV and hot-wire were used for flow measurement in order to further understand the flow control mechanism behind the noise reduction. Three configurations of plasma actuators were investigated, tangential wind actuation (PA1), downward wind actuation (PA2), and spanwise wind actuation (PA3). The noise results suggest that plasma actuator (PA1) is less effective for vortex shedding tonal noise reduction compared with the other configurations. On the other hand the second tested configuration (PA2) showed ability to attenuate vortex shedding tonal noise by 15 dB at 7.5 ms^{-1}. While the last configuration (PA3), demonstrate the ability to reduce the tonal noise by 8dB. In addition, hot-wire and PIV results revealed that the generated electric wind under the current experimental conditions does not eliminates the vortices, but reduces their strength, makes them extended, and reduces the turbulence intensity in the wake region which leads to a reduction in the fluctuating component of the drag coefficient.

Nomenclature

b	=	flat plate span, mm
C	=	chord length, mm
f	=	applied frequency, KHz
H	=	plate height, mm
I	=	input current, mA
l	=	electrode spanwise length, mm
t	=	electrode thickness, mm
U_∞	=	free stream velocity, ms^{-1}
u	=	instantaneous streamwise velocity, ms^{-1}
u_{rms}	=	Root mean square velocity, ms^{-1}
V	=	applied voltage, kV
v	=	instantaneous lateral velocity, ms^{-1}
w	=	Electrode width, mm
ω_x	=	x- component of vorticity, s^{-1}
ω_z	=	z- component of vorticity, s^{-1}

[1] PhD Student, Department of Mechanical, Aerospace and Civil Engineering, Laith.al-sadawi@brunel.ac.uk. member AIAA.
[2]Senior Lecturer, Department of Mechanical, Aerospace and Civil Engineering, t.p.chong@brunel.ac.uk. Member AIAA.

I. Introduction

The unsteady flow structure behind a bluff body, or a body with blunt trailing edge, has been studied extensively due to its importance in many engineering applications. The separation of the free shear layer from the sharp corners of the blunt trailing edge, for example, can lead to formation of vortices that shed alternately from each side of the body. These periodically coherent vortices along with the unsteady velocity field will produce force loading that could increase the aerodynamic drag and reduce the life-expectancy of the flow bodies. In addition, the radiation of narrowband tone noise as a result of the bluntness-induced vortex shedding is a prominent problem in the civil aviation and wind turbine industries. Research efforts are continuously needed to mitigate this type of noise source. Because the radiated aerodynamic noise is a by-product of the flow structure behind the blunt trailing edge or bluff body, one can apply control technique to stabilize the wake flow and reduce the level of noise radiation, simultaneously.

There are numerous studies that aim to control the unsteady flow behind blunt bodies by modifying or suppressing the coherent structures in the wake region, which could be achieved by either the Passive Flow Control (PFC) or Active Flow Control (AFC). The well-documented method of using splitter plate with different gap ratios behind the bluff body can be found in [1-5]. Roshko[5] demonstrated that a splitter plate with length 5 times the cylinder diameter could lead to a total suppression of vortex shedding behind a bluff body and a reduction in the base drag. Roshko also shows that varying the gap ratios of the splitter plate between 0 and 1.75 times the cylinder diameter will result in an extension to the shear layers to the downstream edge of the splitter plate, thus preventing the entrainment of the outer flow to the base region. It is also shown by Liu et al [6] that applying the porous coating on tandem cylinders can lead to stabilization of the vortex shedding from the upstream cylinder, which then reduces the level of wake impingement with the downstream cylinder. The authors suggest that the modified flow field will lead to reductions in the wake vortex shedding noise radiated from the upstream cylinder, as well as the interaction noise with the downstream cylinder. A general review of the PFC technique on the suppression of vortex shedding behind bluff body can be found in Choi et al[7]. Using small element near the trailing edge of a rectangle cylinder at low Reynolds number, Chen et al[8] found that these element successfully suppress vortex shedding and reduces lift and drag fluctuation. Although many of these PFC methods are popular due to their simplicity and ease of implementation, they usually require geometrical modification or attachment of moving or fixed part to the main body. As a result, they are not very versatile when the flow conditions can change considerably over a short period of time.

The improvement in control and electrical technologies in the last decades encourages the development of the AFC. The miniaturization of the actuators also means that very little parasite drag is produced when they are attached to the flow body. The AFC techniques both in the open and closed loop modes can adapt to various flow conditions, thus allowing the user to switch them on and off easily. To attenuate the bluntness-induce vortex shedding, one could seek to prevent the cross-talk between the two separated shear layers, as well as to promote a faster break-up of the coherent structure in the near wake region. Both of which could be achieved by several AFC approaches. Using steady suction and blowing, Henning and King[9] showed that the spanwise coherence of the vortex sheet that sheds from a D-shaped elongated body could be modified. For the same set up, piezo-fluidic actuators were utilized to control the stability of the free shear layer. Despite the robustness and flexibility of the blowing/suction, oscillation and micro-electromechanical, they still possess some disadvantages. These include the complexity of the control system, the need for external power source and the increased overall weight.

More recently, many studies have focused on a promising AFC technique that could alleviate some of the disadvantages described above. The Dielectric Barrier Discharge (DBD) plasma actuator is simple, robust, light-weight, high frequency response and low-power consumption in the unsteady operation mode. It has been demonstrated in many studies that placing single or multiple DBD plasma actuators close to the separation point of an airfoil can prevent the flow separation and increase the lift coefficient[10, 11]. Post and Corke[10] show that the plasma actuator can also prevent flow separation and the formation of dynamic stall vortex for an oscillating airfoil. More interestingly, reduction of turbulent boundary layer skin friction can be achieved by spanwise actuation of the DBD plasma actuators in the same control principle as the mechanical spanwise oscillation[12].
Nati et al [13] successfully suppress the vortex shedding from blunt trailing edge profiled body in the laminar region using different plasma actuator configurations. The study shows that the plasma actuator with downward actuation could effectively suppress vortex shedding at a free stream speed up to 10 m/s. The mechanism of flow control of the aforementioned configuration is by producing stream wise jet that could prevent the cross talk between the separated shear layers and adding momentum in to the wake region. The current study will focus on noise control of a flat plate (in the turbulent region) with blunt trailing edge of 6 mm thickness at different free stream speeds ranging from 7.5 to 40 m/s.

Plasma actuators basically consist two electrodes, one is exposed to the air to which high voltage is supplied from an Alternative-Current (AC) high-voltage power supply; and another electrode is grounded or encapsulated, and is usually covered by either single or multiple layers of dielectric material, which can be

Teflon, Kapton, ceramic and so on. The purpose of the dielectric material is to prevent arc-occurrence between the two electrodes, and to allow for discharge accumulation near the exposed electrode[13, 14]. When high AC voltage of ~ kV with typical sinusoidal waveform, and high frequency of ~ kHz are supplied, strong electric field is generated between the two electrodes. This leads to the creation of ionized region that contains approximately equal numbers of ions and electrons[15]. A body force will then be generated because of the collision between the generated ions and neutral particles. This, in turn, produces an electric wind propagating as a surface jet parallel to the flow direction. As a general rule, higher level of the applied voltage can generate stronger electric wind.

For a flat plate with blunt trailing edge, the separation of the shear layer leads to the creation of spanwise vortices and roll up of the shear layer. This in turn generates high amplitude, narrowband tonal noise. The aim of the current study is to investigate the use of single DBD surface plasma actuators to suppress the vortex shedding in the wake, thereby reducing the narrowband tonal noise. The control strategy is similar to the approach by Nati et al.[13] to disrupt the communication between the separated free shear layers on both sides, or to add momentum into the recirculation region directly. The flat plate has an elliptical leading edge, but two types of trailing edges were investigated. The flat plate is placed at zero incidence with relative to the free stream flow direction. In this paper, the results will be divided into two parts: the acoustics spectra from the noise measurements, and flow measurement obtained by the hot-wire anemometry (HWA) and Particle Image Velocimetry (PIV) techniques. The paper aims to quantify the level of tonal noise reduction by the DBD technique different Reynolds numbers, as well as to understand the physics behind the mechanism of vortex shedding suppression by the plasma system.

II Experimental setup

A. Aeroacoustic wind tunnel Facility and measurement Techniques

Both free field measurements of the flat plate noise and flow tests were conducted in the aeroacoustic wind tunnel at Brunel University London. Fig. 1 shows the aeroacoustic facility where the tests were carried out. This facility includes a hem-anechoic chamber with dimensions of 4 m x 5 m x 3.5 m and a nozzle that is situated inside the chamber and has a rectangular exit section with a dimension of 10 cm (height) x 30 cm (width) and can produce free jet speed of maximum 80ms^{-1} with potential core turbulence intensity between 0.1-0.2 % [16]. The range of the Reynolds numbers investigated in the current study are from $7x10^4$ to $4x10^5$ (chord length of the flat plate is 0.15 m and the freestream velocity ranges from 7.5 to 40 ms^{-1}). A centrifugal fan positioned outside the anechoic chamber is used to generate the air flow that is acoustically treated by a 10 m long silencer, which is located on the roof of the chamber. The tested models can be fixed by two side plates extending from the nozzle.

As shown in Fig. 2, the flat plate has a 0.3 m span and a changeable blunt and rounded trailing edge of 6 mm bluntness height, H. The effect of the plasma actuator on the trailing edge spanwise vortex shedding tonal noise was investigated. The plate has an elliptical leading edge, where both sides of the flat plate were artificially tripped in to turbulent boundary layer using rough sandpaper. As illustrated in Fig. 3, three plasma actuator configurations were investigated in the current study. They were named according to the generated electric wind: the first one is the actuator that generates a tangential electric wind (PA1), the second is the one generates electric wind in the vertical direction along the blunt or the rounded trailing edge height (PA2), while the third one is the actuator that produces wind in the spanwise direction (PA3). The dielectric material used throughout the experiment is the Kapton tape, which has a high dielectric strength. In addition, the material used for both the exposed and covered electrode is copper tape. Table1 summarizes the dimensions of the three configurations of the plasma actuator PA1, PA2, and PA3. Both PA1 and PA2 are situated at the trailing edge of the flat plate, while PA3 is 4mm away from the trailing edge in the upstream direction. A high AC power supply (MiniPulse 6) is used to provide the required voltage to the exposed electrode. This power supply is capable of generating up to 60 kV peak to peak sinusoidal waveforms. A signal generator (LeCroy wave station) is used to produce a square wave as an input signal to drive the voltage supply. The range of the voltage tested in the current study is from 3kV to 7.5 kV.

The far field noise measurements were conducted using a ½ inch free field type pre-polarized condenser microphone (LarsonDavis 377B02). The microphone is installed at distance of 1 m above the mid span of the flat plate. A 16 bit analogue-digital card was used to sample the noise data at a sampling frequency of 44 KHz, after that the power spectral density was obtained by averaging the windowed FFT with a resolution of 1 Hz. In addition, an acoustic camera was used to predict the noise source and to confirm the measured noise data taken by the microphone. The acoustic camera is composed of 16 microphones that are distributed evenly around a circular ring and a camera located in the center of the microphone ring. Both the camera and the microphones are connected to the data acquisition system and can be controlled from the pc.

To investigate the mechanism of noise reduction by the plasma actuators, hot wire anemometry (HWA) and particle image velocimetry (PIV) were utilized for flow measurements. Both the hot wire and PIV measurements were taken place downstream of the flat plate trailing edge to determine the flow structure in the wake region with and without the plasma control. A glass pitot tube, which has an outer diameter of 1.2 mm and an inner diameter of 1 mm, was used to measure near wake mean velocity profile instead of using the hot wire to avoid arching between the plasma discharge and metal prongs of the hot wire probe. The pressure was sensed by a pressure transducer type (HCXM010D6H) that has a differential pressure ranging from 0 to 10 mbar. The reference pressure (ambient pressure) was measured by another tube that was positioned far from the trailing edge. The instantaneous velocity profile and velocity spectral density was measured by a single type hot wire probe that was situated at distant of 25 mm from the trailing edge. The hot wire probe type is DANTEC 55P11 that is connected to constant temperature anemometer (CTA) (DANTEC 55M01). The probe is connected to a two-directional traverse system that has accuracy of 0.01 mm in both directions.

The velocity field near the trailing edge of the flat plate in the wake region was measured by the PIV technique. The PIV system includes a source that generates a double pulse laser beam (Litron® Nd:YAG-Laser) with maximum output energy of 800 mJ. The laser beam has a diameter of 5 mm that can be expanded through a set of lenses. The maximum pulsing frequency is 15 kHz and the time between the two pulses is 10 μs. A CCD camera (FlowSense EO 2M) is used to capture the images of the flow domain. This camera is able to capture 44 frames per seconds (FPS) with output resolution of 1600 x 1200 pixel, which have size of 7.4 μm. Polyethylene glycol (PEG) oil was used as seeding fluid because of its good reflection characteristics at high laser intensities. The oil droplet has an average diameter of 2 μm which was seeded via a pressurized oil chamber (Dantec High Volume liquid Droplet Seeding Generator) and injected upstream of the nozzle outlet section. Conventional cross correlation algorithm was used on 32 x 32 pixel grid to calculate the velocity vectors from the peak correlation of group of particles using the DynamicsStudio software. The average velocity was computed by averaging approximately 140 images of the instantaneous velocity distribution. Because of laser reflection from the exposed electrode of the plasma actuator (the copper has a shining surface), the PIV results are not accurate in this region compared to the main flow region. In the current study, the measurement planes comprise of two configurations: the first is the XY plane where the camera was perpendicular to the streamwise direction for both the PA2 and PA3 actuators. The second plane is the YZ plane, where the camera was parallel to the spanwise direction to visualize the development of the spanwise vortices that are generated by the spanwise actuation.

III Results

This result section will be divided into two parts: Section III.A describes the acoustic data, which include the acoustic power spectral density and noise source identification. Section III.B will present the flow data that include the mean wake velocity/turbulence profiles, fluctuating velocity power spectral density, flow vector and magnitude and vorticity.

A. Acoustics results

The noise data for the flat plate model (blunt and the rounded trailing edges) with the three plasma actuator configurations PA1, PA2, PA3 are discussed. The effects of different operating parameters such as the dielectric thickness, applied frequency and input voltage were first examined in order to determine the optimal values. The performance index was based on the Overall Sound Pressure Level (OASPL), which is calculated by integrating the acoustic pressure fluctuation over a finite frequency range (130 to 290 kHz). These frequency limits correspond to the upper and lower limit of the narrowband vortex shedding tonal noise, respectively. Figure 4 demonstrates the effect of the number of the dielectric layers on the ΔOASPL over input voltages of 3 to 7.5 kV, and an applied frequency of 8 kHz. Note that ΔOASPL is the difference in noise level between the "plasma off" case and the "plasma on" case. Therefore a positive ΔOASPL represents narrowband noise reduction, and the opposite is true. It can be seen that as the input voltage increases the ΔOASPL increases. The largest noise reduction was achieved at the input voltage of about 5.5 kV with 3-4 layers of the dielectric film. Although 3-4 layers of the dielectric film produces the largest noise reduction, 5 layers of dielectric film was eventually chosen due to the better resistance in structural damage by the high voltage input.

The performance of each plasma configuration PA1, PA2 and PA3 was first investigated. Figure 5 shows the sound pressure level (SPL) produced by the flat plate (with blunt trailing edge) with and without plasma actuations. The plasma configuration is the PA1 type. The operating configuration covers the applied voltages from 2.4 to 4.2 kV and two excitation frequencies, 7 and 8 kHz. The freestream velocity was set at 7.5 ms^{-1}. The noise spectra in Fig. 5 use the blunt height, H, as the length scale to provide a dimensionless frequency. A strong tonal peak clearly appears for the baseline, "plasma off" case at $fH/U \approx 0.199$. This indicates that this tonal peak relates closely to vortex shedding tonal noise due to the blunt trailing edge. When the PA1 plasma actuator is

activated at applied voltages ranging from 2.4 to 3.6 kV, the vortex shedding peak still exists. A small noise reduction of about 1 and 1.9 dB is obtained at the maximum applied voltage of 4.8 kV at the applied frequencies of 7 and 8 kHz, respectively. The tones are also observed to slightly shift to a higher frequency. This is possibly an indication that the induced plasma jet has reduced the length scale of the vortex wake structure [11].

The effectiveness of the plasma actuator PA1 was explored at higher velocities. Figure 6 shows the ΔSPL contours as a function of the freestream velocity and frequency. Note that ΔSPL is the difference in SPL between the "plasma off" case and the "plasma on" case. A positive ΔSPL therefore denotes noise reduction, and vice versa. From the figure, three characteristic regions can be identified, which are bounded by the upper and lower limit of the narrowband vortex shedding tonal noise. The level of +ΔSPL of this narrowband frequency increases as the input voltage increases, but only occurs at the freestream velocity between 7.5 and 15 ms^{-1}. No noise reduction was observed at the input voltages lower than 4.2 kV and the effectiveness of the PA1 deteriorates at higher freestream velocity. In the high frequency region, a distinct noise peak (-ΔSPL) appears due to the self-noise generated by the plasma actuator. These noise peaks occur at the subharmonic frequencies of the plasma excitation frequencies.

The investigation continues with another type of plasma configuration: PA2. The corresponding SPL spectra for both the "plasma off" and "plasma on" cases are shown in Fig. 7. The freestream velocity was set at 7.5 ms^{-1}, and the input voltages range from 2.4 to 4.8 kV with two applied frequencies 7 and 8 kHz. The figure shows that increasing the input voltage lead to significant suppression of the vortex shedding tonal noise, with a maximum reduction of 15 dB achievable at the highest input voltage (4.8 kV) and excitation frequency of 8 kHz. At lower input voltage (e.g. 3.6 kV), the radiated tonal peak as a results of the PA2 plasma is also shifted to a higher frequency, indicating the reduction in wake vortex length scale. Figure 8 shows the ΔSPL contours at freestream velocity between 7.5 and 40 ms^{-1} under two excitation frequencies of 7 and 8 kHz. Similarly, the level of +ΔSPL by the PA2 is represented in the mid frequency region (between the dashed lines), from which it is clear that as the voltage increases the +ΔSPL level become larger. There is no clear distinction between the excitation frequencies of 7 and 8 kHz for the plasma actuator. The velocity range which the PA2 plasma actuator is effective is also larger (tonal noise reduction effective up to 25 ms^{-1}).

The third plasma configuration, PA3, should produce an electric wind in the spanwise direction. The corresponding SPL spectra for the "plasma off" and "plasma on" cases at free stream velocity of 7.5 ms^{-1} are shown in Fig. 9. When the PA3 plasma is activated at an input voltage of 3 kHz, the narrowband vortex shedding noise was reduced by about 8 dB and 7.7 dB at 6 and 7 kHz, respectively. One interesting observation is that the tone peak frequencies do not shift under the PA3 plasma configuration, which is different to both the PA1 and PA2 cases.

The PA2 plasma configuration has been shown to provide the best noise reduction capability among the three configurations. A flat plate with a rounded trailing edge that has a radius equal to half the plate height (H/2) was also examined with the PA2 plasma set up. The corresponding SPL results between the "plasma off" and "plasma on" cases are shown in Fig 10 for freestream velocity of 7.5–20 ms^{-1}. The PA2 plasma actuator coupled with the rounded trailing edge lead to vortex shedding noise reduction of about 12 dB at freestream velocity of 7.5 ms^{-1}. However, at free stream velocity of 10 ms^{-1}, a larger level of tonal noise reduction of about 15.8 dB is produced. It is not clear yet why such an opposite trend occurs, and more repeatability tests need to be conducted to confirm this. Further increase of the freestream velocity to 15 and 20 ms^{-1} decrease the effectiveness of the plasma actuator, achieving 8.4 and 4 dB reduction, respectively. The tonal peaks are shifted to higher frequency, presumably due to the reduction in the length scale of the wake vortex structure.

Finally, an acoustic camera were utilized to identify the noise source and to check the magnitude of the narrowband noise reduction using the PA2 plasma actuator. Figure 11 shows the noise image of the blunt trailing edge flat plate for both the "plasma off" and "plasma on" cases. The results show that the noise source is near the trailing edge of the flat plate. When the PA2 plasma actuator is turned on, the vortex shedding tonal noise was reduced at 900 Hz by about 1 dB at free stream velocity of 30 ms^{-1}. Figure 11 supplements what is previously obtained from the single microphone results, which show that the main noise source is the trailing edge self-noise and the vortex shedding tonal noise in the wake.

B. Flow results

1. Pitot tube and hot-wire (mean velocity profile and fluctuating velocity power spectral density)

This section will investigate the flow fields as the result of the activation of the plasma actuators. The flow measurements were mainly carried out at an input voltage of 4.2 kV and excitation frequency of 8 kHz to the plasma actuators. To avoid the arcing between the hot wire probe and the plasma discharge, the wake velocity profile measurements were made by traversing a glass-type Pitot tube for sections close to the trailing edge. Figure 12a shows the mean velocity profile at a downstream position of X = 1 mm from the blunt trailing edge

in the very near wake region. When the plasma actuator is off, the wake region has a dead air pocket because the separating shear layers on both side of the trailing edge have not fully mixed yet. For the "plasma on" case, a small streamwise velocity representing a plasma jet (ionic wind) is generated at the plate centreline. The ionic wind velocity depends on the applied voltage, i.e. the higher the input voltage the higher the generated ionic wind velocity until reaching a saturation limit of the voltage, in which case the plasma actuator will no longer produce higher ionic wind and a breakdown of the plasma system may occur. Further downstream at $3 \le X \le 7$ mm from the trailing edge, the induced jet by the plasma actuator decays quite rapidly. The resulting velocity profiles thus resemble very closely to the "plasma off" case. It can also be seen that the dead air pocket is still prominent at X = 7 mm for both the "plasma off" and "plasma on" cases. The results in Fig. 12 are therefore quite remarkable. Although the wake profiles do not seem to be very different, significant narrowband noise reduction has been produced under the same plasma setting (see Fig. 7). This issue will be further investigated in the next section when the PIV results are discussed.

Hot-wire measurements were made to investigate the fluctuating velocity spectral density for both the "plasma off" and "plasma on" cases at X = 25 mm, and Y = -7 mm. As shown in Fig. 12, it can be seen that a narrowband vortex shedding occurs at the same frequency (257Hz) observed in the acoustic spectrum. The results demonstrate that a reduction in the vortex shedding peak, as well as the broadband component at higher frequency, can be achieved when the PA2 plasma actuators are turned on. Because the u_{rms} (root-mean-s1uare of the velocity fluctuation) can be obtained by integrating the fluctuating velocity spectral density across the frequency range, the result demonstrates that the turbulence intensity in the wake can also be reduced. However, this becomes less effective at further downstream positions.

2. PIV (velocity vector and magnitude and vorticity)

The PIV results will be presented in two parts: the first one is the results of blunt trailing edge flat plate with the PA2 plasma actuator in quiescent condition. The second part of the results will focus on the effect of the induced jet by plasma actuator and its effect on the wake vortex shedding at freestream velocity of 7.5ms^{-1}. Figure 14 shows the streamwise induced velocity by the plasma actuator PA2 at quiescent condition at an input voltage of 4.2 kV and excitation frequency of 8 kHz. The plasma actuator under these operating conditions can generate an ionic wind with maximum velocity of 1 ms^{-1} in the current setting. Note that this value is less than the induced velocity produced by Nati et al [12] because they operated their plasma actuators at a much higher input voltage (peak-to-peak) of 18 kV and 2 kHz. Another plasma configuration PA3 (spanwise actuation) was also investigated in the quiescent condition. Figure 15 shows velocity contours of the spanwise actuation of the PA3 in quiescent condition. The results of the velocity contours indicate that spanwise actuation produces a normal jet with a similar maximum velocity of 1 ms^{-1}. The PA3 plasma can also produce series of counter-rotating spanwise vortices, as shown in Fig. 16 for the vorticity contour. Comparing the Figs. 15 and 16 demonstrates that the induced jet (upward) will encourage entrainment of fluids towards the wall on both sides.

The effect of the plasma actuator PA2 on the near wake region (freestream velocity = 7.5 ms^{-1}, 4.2 kV and 8 kHz) is shown in Fig. 17. The figure demonstrates the mean velocity contours behind the blunt trailing edge. For the "plasma off" case, a re-circulating air pocket features prominently up to X/H ≈ 1.5, which agrees well with the previous wake profile measurement where no velocity was detected at the centerline at X = 7 mm or X/H = 1.17 (see Fig. 12d). Interestingly, for the "plasma on" case, the re-circulating air pocket seems to extend farther than the "plasma off" case.

By examining the very near wake region, as in Fig. 12a for X = 1 mm or X/H = 0.17, there is a plasma jet produced at the centerline of the blunt trailing edge, as well as some near the blunt edge on both sides. Note that this very near wake is not accessible by the PIV result as light reflection occurs at this region. Due to these induced air jet at the centerline and the blunt edges, the re-circulating air pocket will tend to be more slender than the "plasma off" case. The vortical structure behind the flat plate presented in Fig. 18 shows that activation of plasma actuator lead to extension of the shear layer in the streamwise direction compared with plasma off case. The effect of the plasma actuation on the turbulence Intensity in the wake region is shown in Fig. 19. The result shows that both streamwise turbulence intensity and vertical one has been reduced in the three tested positions (3, 5, and 7 mm) from the base of the flat plate. This, in turn, leads to a reduction in the fluctuating component of the drag, which can be calculated using Eq. (1):

$$C_D = \frac{2}{b*H}\int \frac{u}{U_\infty}\left[1-\frac{u}{U_\infty}\right]dy + \frac{2}{b*H}\int\left[\frac{u_{rms}}{U_\infty}\right]^2 dy \qquad (1)$$

The above equation is based on the methodology described by Naghib-Lahouti et al [17, 18] where b is the span length of the plate and H is its thickness. The obtained results show that the maximum reduction of the fluctuating component of the drag coefficient (the second term in Eq. 1) is about 16% whereas no reduction is achieved in for the mean component of the drag (the first term in Eq. 1). The current results suggest that the

effect of flow control mechanism on the length of vortex formation is obvious at the lowest tested velocity, where the maximum reduction in the second term of eq. 1 is achieved.

The effect of the spanwise actuation (PA3) on the near wake structure of the blunt trailing edge flat plate was also explored in both XY and YZ planes. Fig. 20 exhibits the streamwise velocity component for plasma on and plasma off cases of blunt trailing edge flat plate at free stream velocity of 7.5 ms^{-1}. The results show that when plasma actuator PA3 is switched on, the two symmetric recirculation structures of the baseline case alters and the width of the wake is increased, which is due to the local spanwise vortices generated by the plasma actuator. In order to see the development of the vortices in the YZ plane, three downstream positions were tested, 12 mm upstream the trailing edge of the flat plate, 0 mm at the trailing edge, and 2 mm from the trailing edge in the downstream direction as shown in Fig. 21. The result show that the stream wise vortices are generated when the plasma actuator is switched on and it decay as it goes in the downstream direction.

Because of the superior performance of the PA2 actuator in reducing vortex shedding tonal noise, it selected to investigate its effect on the wake region behind the rounded trailing edge flat plate using the PIV system at free stream velocity of 7.5 ms^{-1}. Fig. 22 shows the contours of the streamwise component of the flow velocity for the baseline case and plasma on cases. The results show that when plasma actuator is on, the width of the wake is reduced and the center of the recirculation behind the flat plate base is moved out in the downstream direction. The vortical structure behavior behind the rounded trailing edge is found to be similar to that of the blunt trailing edge, where the shear layer extended in the streamwise direction compared with baseline (plasma off) case.

IV Conclusion

A blunt and rounded trailing edge flat plate with surface single dielectric barrier plasma actuator has been experimentally investigated. Three different plasma actuator configuration were explored, PA1, PA2, and PA3, which produce tangential, downward, and spanwise ionic wind at Reynolds numbers ranging from $7x10^4$ to $4x10^5$. The aim of the current research is to examine the effect of the plasma actuator on the narrowband tonal noise that radiates from the blunt and rounded trailing edge of a flat plate at zero angle of attack. Both aeroacoustic noise and flow measurements were carried out using free field single microphone and both hot-wire and PIV system respectively. Noise measurements show that plasma actuator configuration PA1 has little effect on the radiated tonal noise, whereas the other configurations PA2 and PA3 show that it can reduce the tonal noise by about 15dB and 8 dB, when operated at (8 KHz, 4.2 kV) and (6 KHz, 3 kV) respectively. For flat plate with rounded trailing edge, results show that the PA2 surface plasma actuator can reduce noise at higher velocities (10 ms^{-1}) by 15 dB. It is also found that the plasma actuator itself produces self-noise at wide range of high frequencies especially at low velocities due to low background noise. In addition, flow measurement represented by pitot tube for regions close to the trailing edge revealed that operating the PA2 surface plasma actuator result in generation of streamwise jet directly into the recirculation region compared with baseline case (plasma off). The unsteady velocity spectra measured by hot-wire shows that not only the vortex shedding narrowband noise was reduced but also the other frequencies were also reduced. This, in turn, results in a reduction in the wake turbulence intensity that is confirmed by PIV measurements. Quiescent condition PIV results show that the PA2 plasma actuator can induce streamwise jet with velocity found to be slightly less than $1.2ms^{-1}$. Although, Nati found that the flow control mechanism is by addition of momentum directly in to the wake region when the actuator is operated at high voltage 18 kV and low frequency, 2KHz, It is found here that the current plasma actuator can reduce noise at lower voltages and the possible reason for that is due to prevention of the interaction between the two separated shear layers from both sides of the flat plate. Moreover, the turbulence intensity calculated by the PIV suggests that plasma actuator (PA2) can reduce both lateral and streamwise turbulence intensity at three tested positions, 3, 5, and 7 mm and thus reduces the fluctuated component of the drag coefficient. On the other hand, the results for the plasma actuator PA3 show that possible mechanism for noise reduction is by producing spanwise counter rotating vortices which can locally increase the mixing between the boundary layer and the outer flow.

IV References

[1] Bailey, S., Kopp, G., and Martinuzzi, R., "Vortex shedding from a square cylinder near a wall," *Journal of Turbulence*, Vol. 3, No. 3, 2002, pp. 1-18.

[2] Jodai, Y., Takahashi, Y., Ichimiya, M., "The effects of splitter plates on turbulent boundary layer on a long flat plate near the trailing edge," *Journal of Fluids Engineering*, Vol. 130, No. 5, 2008, pp. 051103.

[3] Ozono, S., "Flow control of vortex shedding by a short splitter plate asymmetrically arranged downstream of a cylinder," *Physics of Fluids,* Vol. 11, 1999, pp. 2928-2934.

[4] Akilli, H., Sahin, B., and Filiz Tumen, N., "Suppression of vortex shedding of circular cylinder in shallow water by a splitter plate," *Flow Measurement and Instrumentation,* Vol. 16, No. 4, 2005, pp. 211-219.

[5] Roshko, A., "On the wake and drag of bluff bodies," *Journal of the Aeronautical Sciences (Institute of the Aeronautical Sciences),* Vol. 22, No. 2, 2012,

[6] Liu, H., Azarpeyvand, M., Wei, J., & Qu, Z., "Tandem cylinder aerodynamic sound control using porous coating". *Journal of Sound and Vibration,* Vol. 334, 2015, pp. 190-201.

[7] Choi, H., Jeon, W., and Kim, J., "Control of flow over a bluff body," *Annu.Rev.Fluid Mech.,* Vol. 40, 2008, pp. 113-139.

[8] Chen, Y.J., and Shao, C.P., "Suppression of vortex shedding from a rectangular cylinder at low Reynolds numbers," *Journal of Fluids and Structures,* Vol. 43, 2013, pp. 15-27.

[9] Henning, L., and King, R., "Drag reduction by closed-loop control of a separated flow over a bluff body with a blunt trailing edge," *Decision and Control, 2005 and 2005 European Control Conference. CDC-ECC'05. 44th IEEE Conference on,* IEEE, 2005, pp. 494-499.

[10] Post, M.L., and Corke, T.C., "Separation control using plasma actuators: dynamic stall vortex control on oscillating airfoil," *AIAA Journal,* Vol. 44, No. 12, 2006, pp. 3125-3135.

[11] Akansu, Y., Karakaya, F., and Şanlısoy, A., "Active Control of Flow around NACA 0015 Airfoil by Using DBD Plasma Actuator," *EPJ Web of Conferences,* Vol. 45, EDP Sciences, 2013, pp. 01008.

[12] Kozlov, A.V., and Thomas, F.O., "Plasma flow control of cylinders in a tandem configuration," *AIAA Journal,* Vol. 49, No. 10, 2011, pp. 2183-2193.

[13] Nati, G., Kotsonis, M., Ghaemi, S., "Control of vortex shedding from a blunt trailing edge using plasma actuators," *Experimental Thermal and Fluid Science,* Vol. 46, No. 0, 2013, pp. 199-210.

[14] Kotsonis, M., and Ghaemi, S., "Forcing mechanisms of dielectric barrier discharge plasma actuators at carrier frequency of 625 Hz," *Journal of Applied Physics,* Vol. 110, No. 11, 2011, pp. 113301

[15] Tonks, L., and Langmuir, I., "Oscillations in ionized gases," *Physical Review,* Vol. 33, No. 2, 1929, pp. 195.

[16] Vathylakis, A., Kim, J.H., and Chong, T.P., "Design of a low-noise aeroacoustic wind tunnel facility at Brunel University," *20th AIAA/CEAS Aeroacoustic Conference and Exhibit,* 2014,

[17] Naghib-Lahouti, A., Doddipatla, L., and Hangan, H., "Flow Control Based on Three-Dimensional Wake Instabilities for a Blunt Trailing Edge Profiled Body," *17th Australasian Fluid Mechanics Conference,* 2010.

[18] van Oudheusden, B.W., Scarano, F., Roosenboom, E.W., "Evaluation of integral forces and pressure fields from planar velocimetry data for incompressible and compressible flows," *Experiments in Fluids,* Vol. 43, No. 2-3, 2007, pp. 153-162.

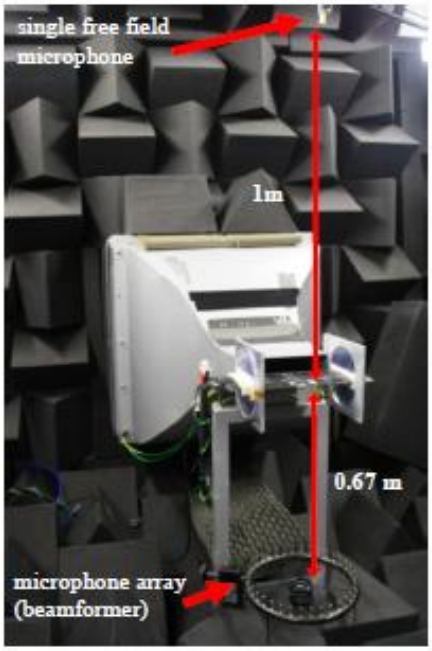

Figure 1. Aeroacoustic facility

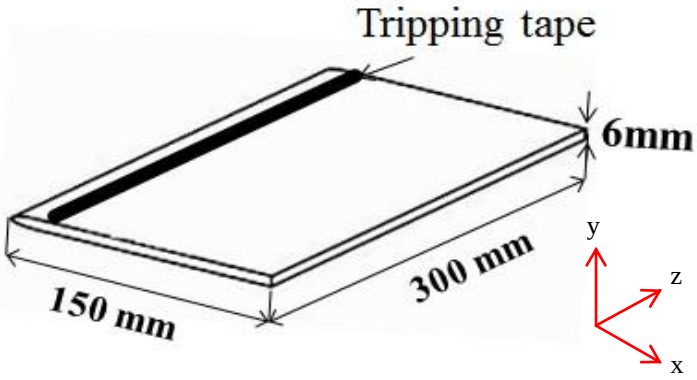

Figure 2. Blunt trailing edge flat plate model.

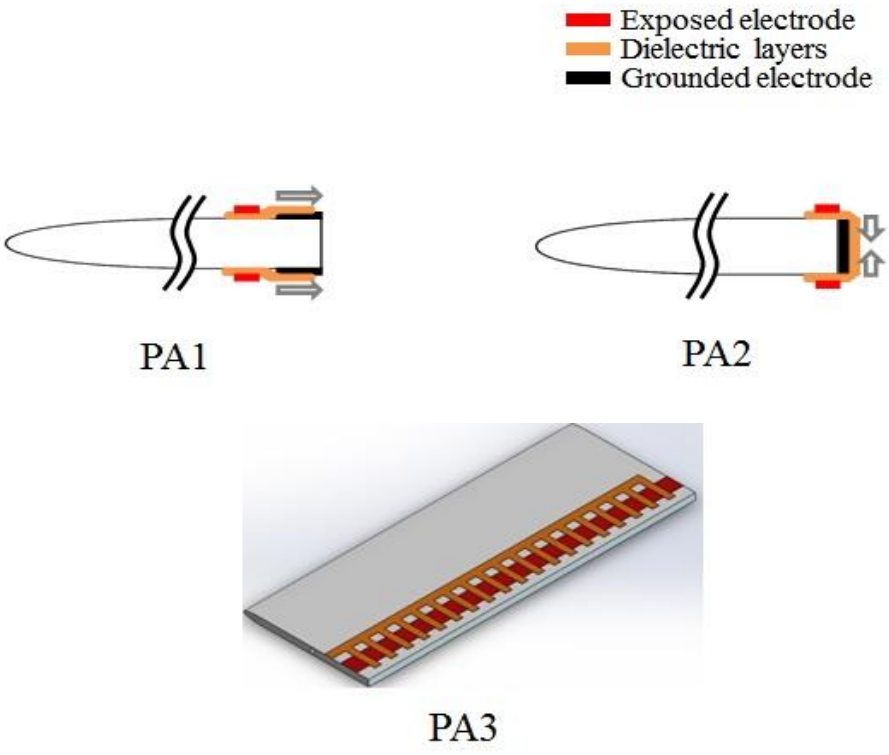

Figure 3. Plasma actuator configurations.

Table 1. The geometric specification of the tested plasma actuators.

Parameter	Value
Exposed electrode, (length, width, thickness)	(280 mm), (6 mm for the three tested configurations), (0.035 mm)
Grounded electrode, (length), (width) and (thickness)	(280 mm), (10 mm for tangential actuator 6 mm for both downward and 150mm for the spanwise actuator) ,(0.035 mm)
Horizontal gap (space between the edge of the exposed electrode and grounded one)	0 mm
Applied frequency, Voltage	6 to 8 KHz , 2.4 to 4.8 kV
Output signal shape	Sinewave signal
Dielectric material (Kapton tape), Thickness	1mil (0.025mm)
Maximum total thickness of the tested actuator	**0.25 mm**

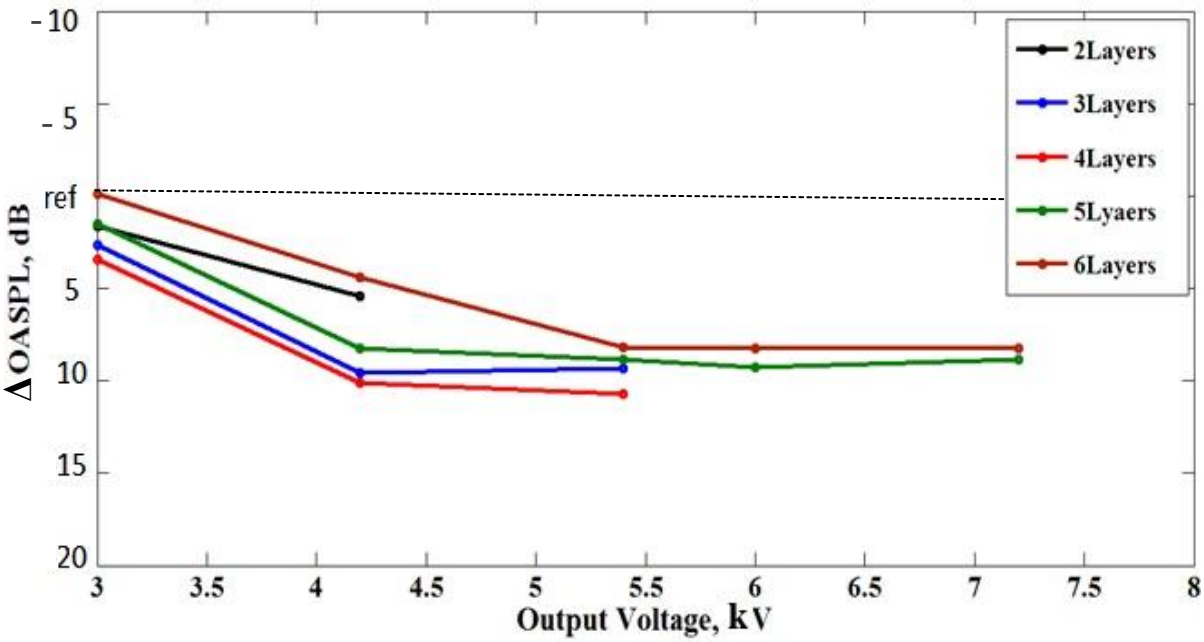

Figure 4. Effect of dielectric thickness on noise reduction by the PA2 Surface plasma actuator.

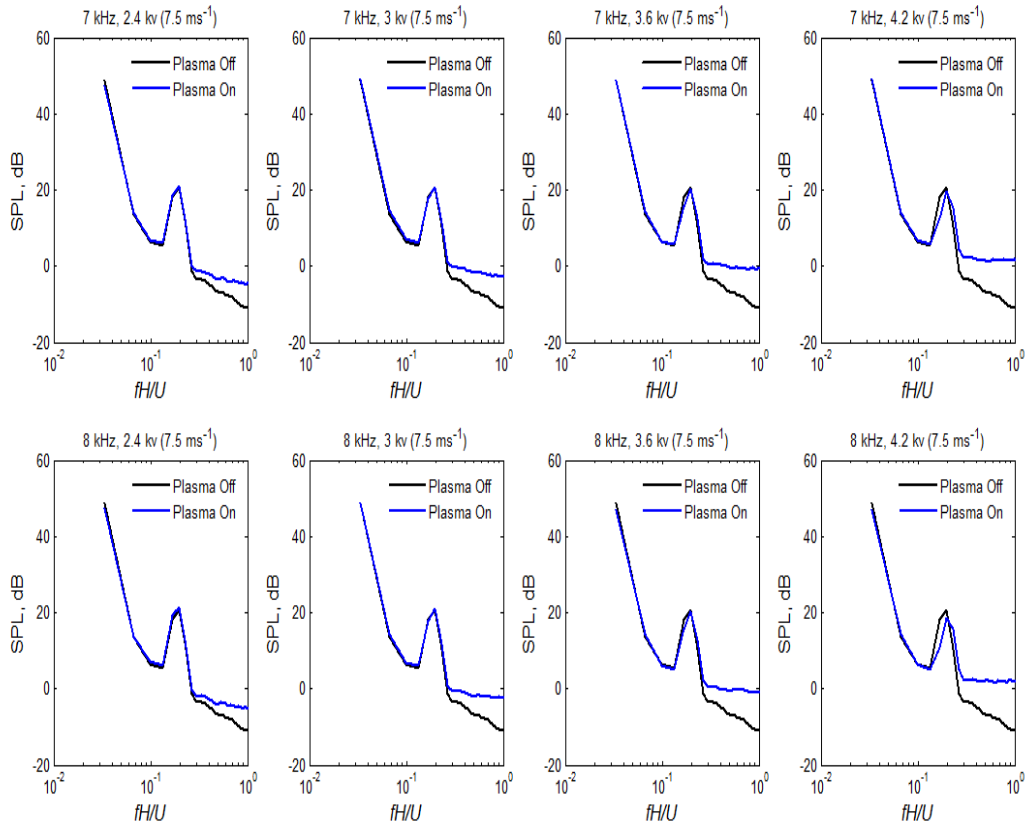

Figure 5. Noise sound pressure level spectra of the PA1 surface plasma actuator at excitation frequency 8 KHz and 7 KHz and free stream velocity of 7.5 ms^{-1}.

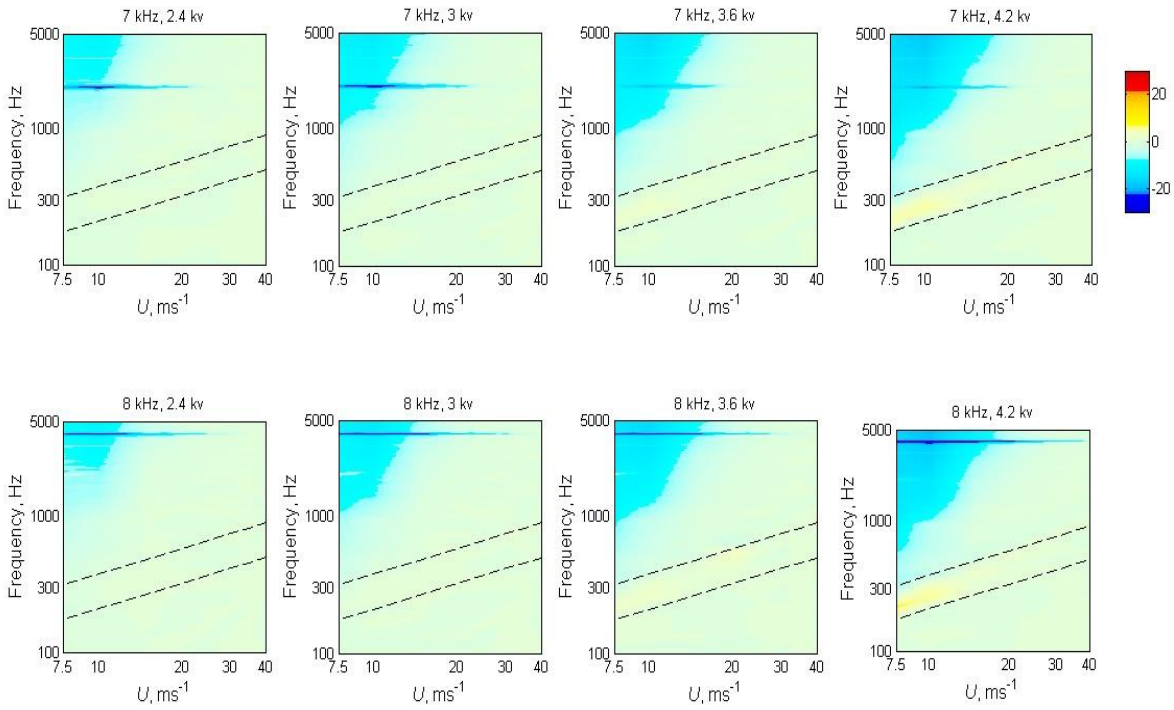

Figure 6. Noise reduction contours of PA1 surface plasma actuator at frequency 8 KHz and 7 KHz and free stream velocity of 7.5 ms^{-1}.

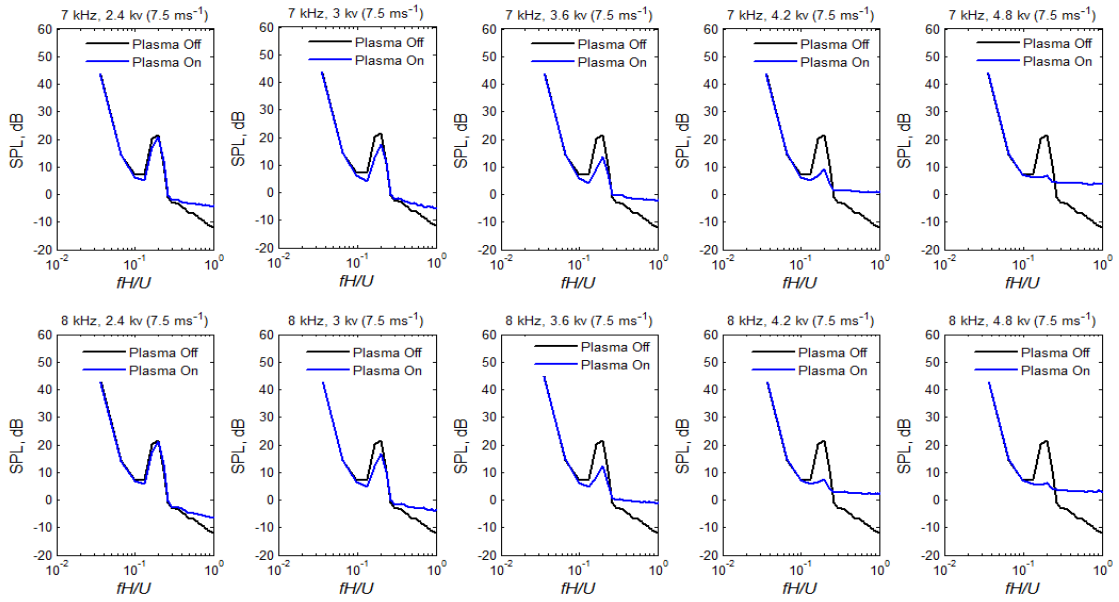

Figure 7. Noise sound pressure level spectra of the PA2 surface plasma actuator at excitation frequency 8 KHz and 7 KHz and free stream velocity of 7.5 ms^{-1}.

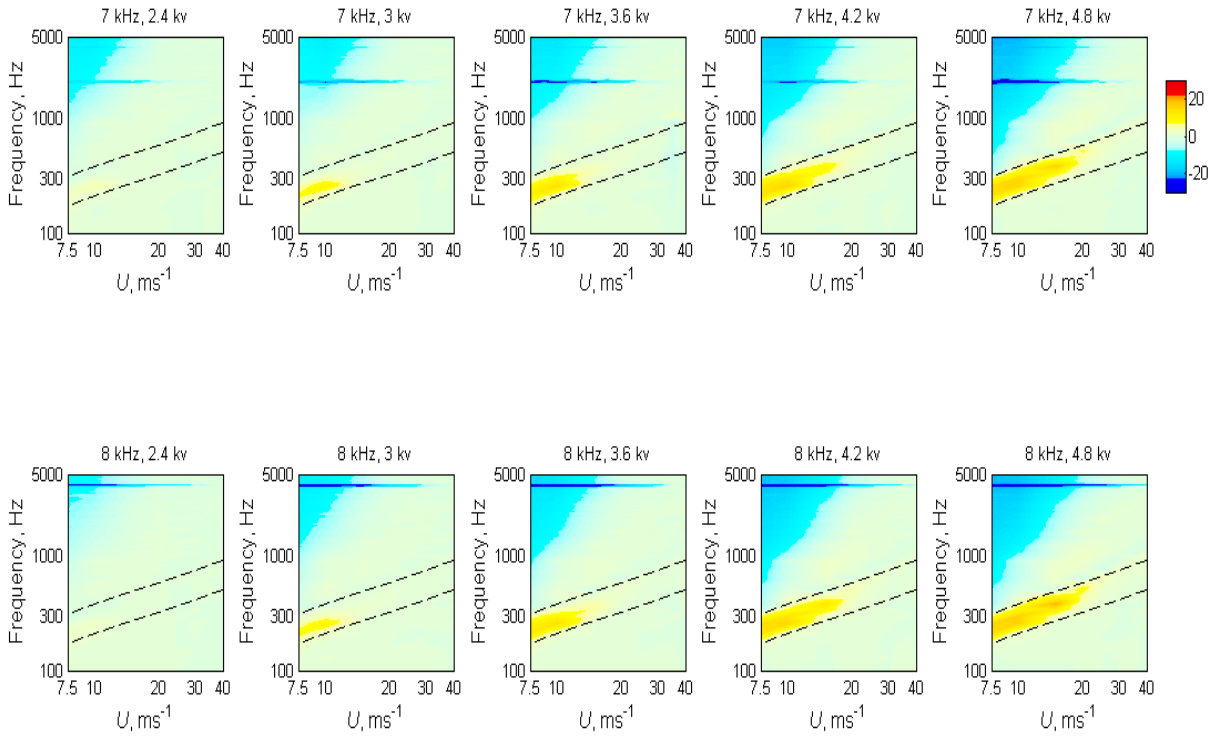

Figure 8. Noise reduction contours of PA2 surface plasma actuator at frequency 8 KHz and 7 KHz and free stream velocity of 7.5 ms^{-1}.

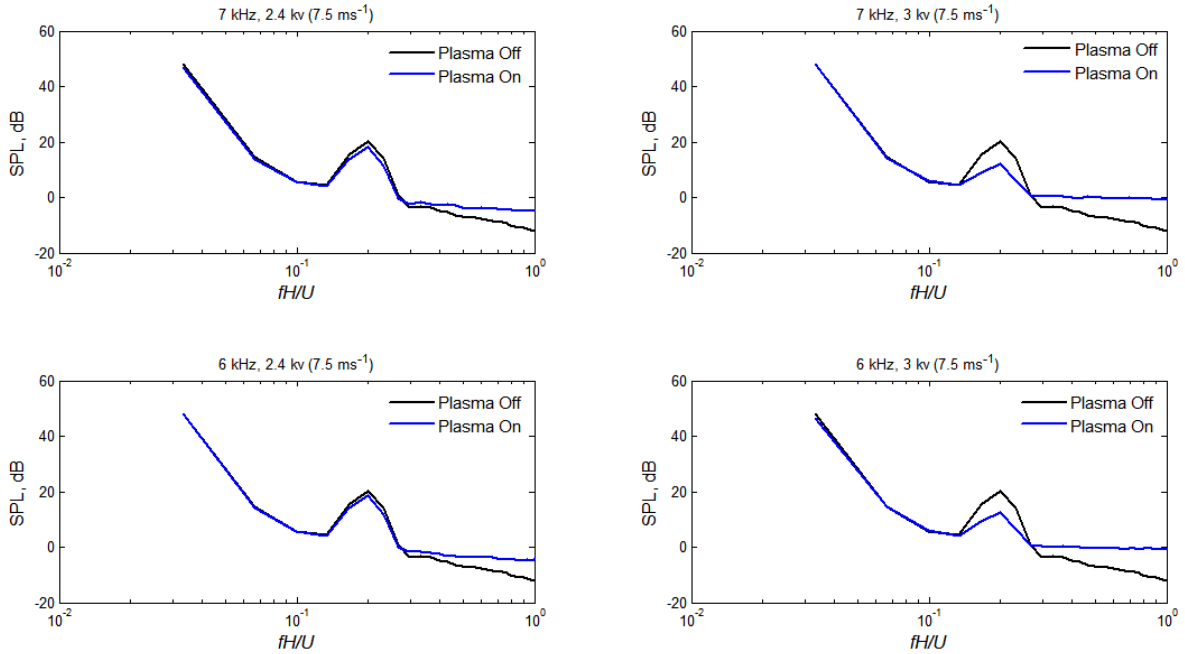

Figure 9. Noise sound pressure level spectra of the PA3 surface plasma actuator at excitation frequency 7 KHz and 6 KHz and free stream velocity of 7.5 ms^{-1}.

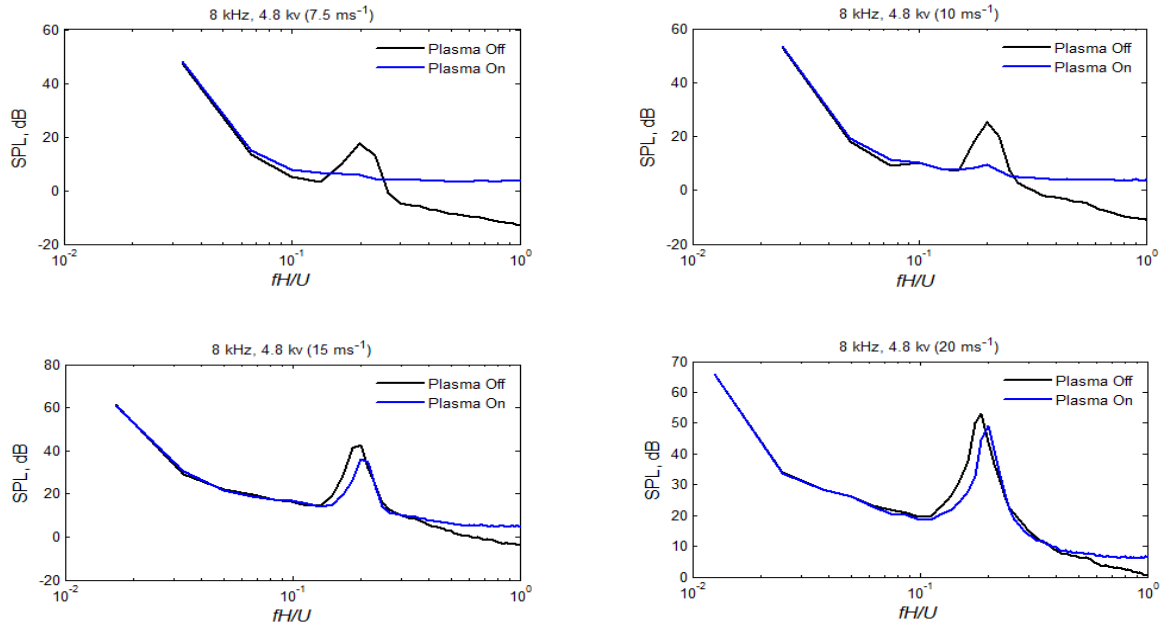

Figure 10. Noise sound pressure level spectra of rounded trailing edge flat plate with the PA2 surface plasma actuator at excitation frequency 8 KHz and free stream velocity of 7.5 ms^{-1}.

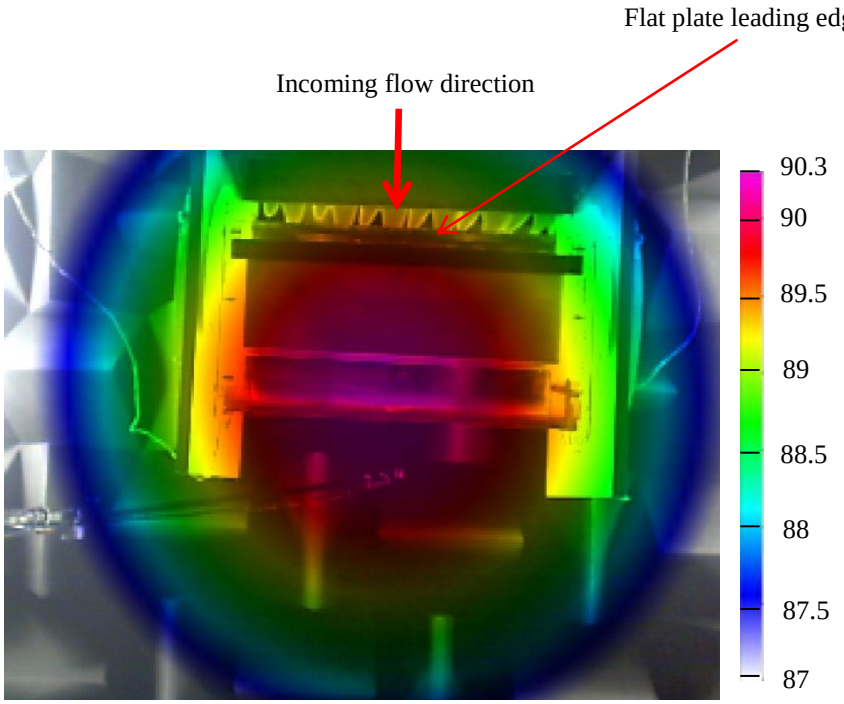

a) Plasma off

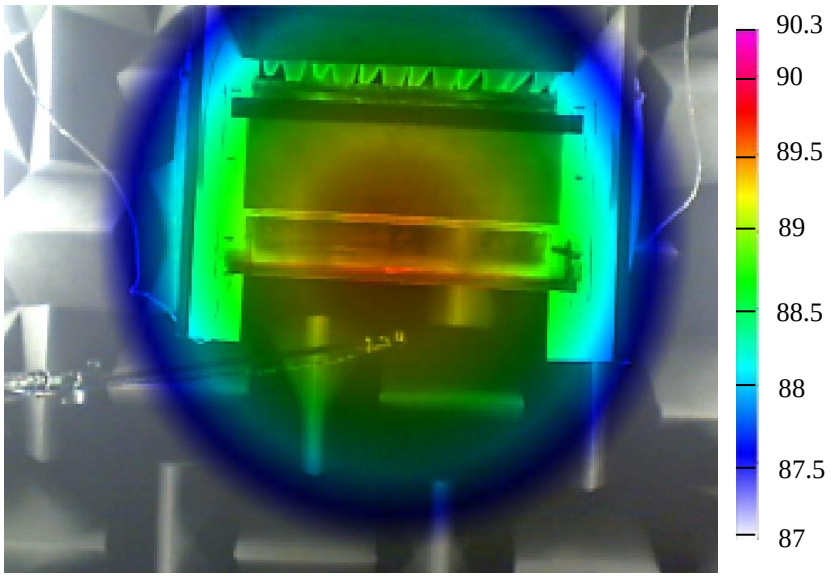

b) Plasma on

Figure 11. Acoustic camera noise Image at tonal peak frequency of 900 Hz and free stream velocity of 30 ms^{-1}.

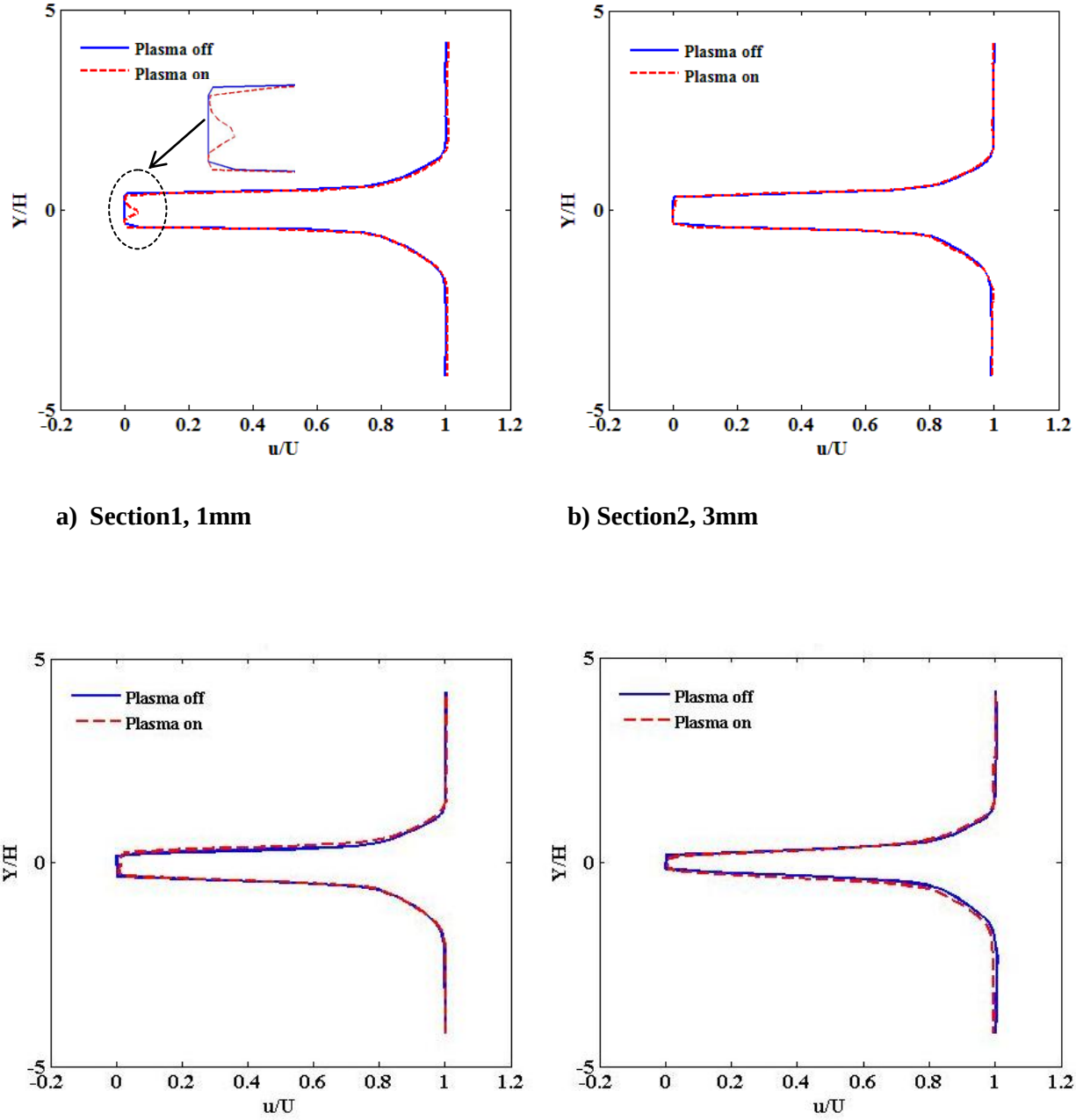

a) Section1, 1mm **b) Section2, 3mm**

c) Section3, 5mm **d) Section4, 7mm**

Figure 12. Mean velocity profile measured by pitot tube at free stream velocity, 7.5 ms^{-1} and different downstream sections (8KHz and 4.2kV).

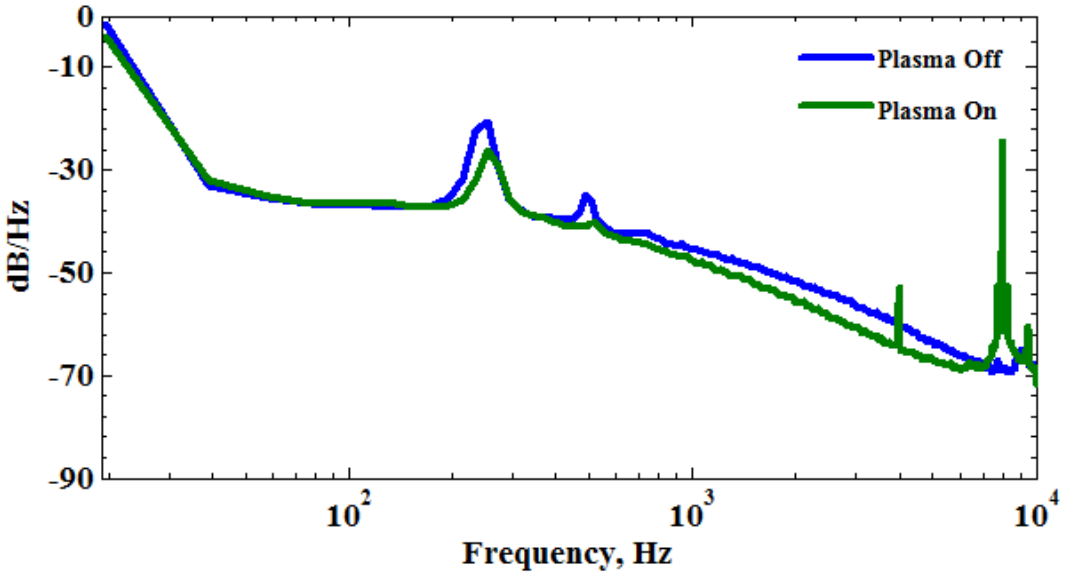

Figure 13. Unsteady velocity wake spectrum for Blunt trailing edge flat plate at free stream velocity of 7.5 ms^{-1}, and applied frequency and voltage 8KHz, 4.2KV and Y= -7mm.

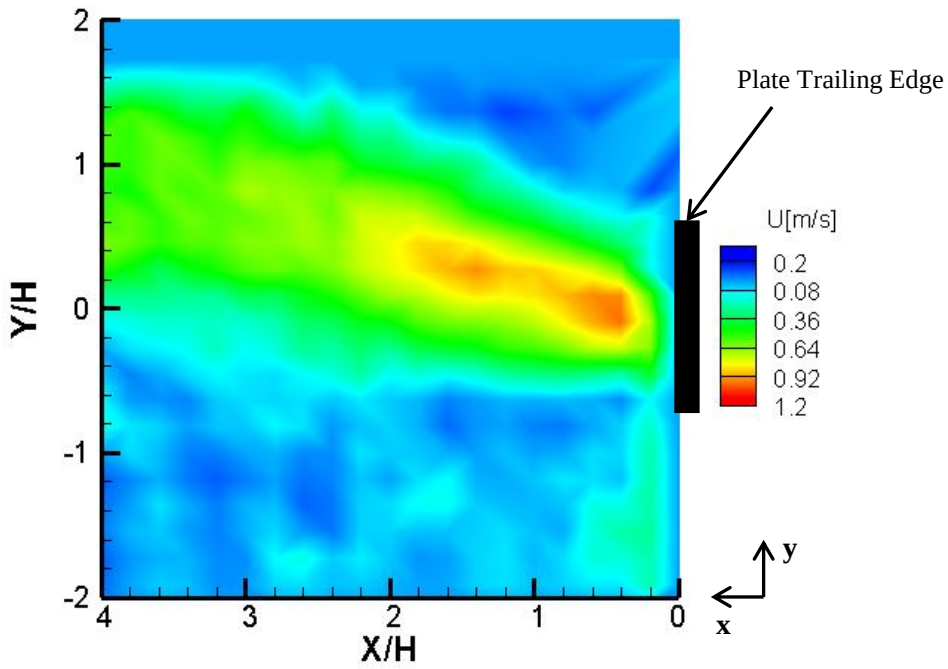

Figure 14. Jet induced by the plasma actuator (PA2) at quiescent condition (8 KHz, 4.2 kV).

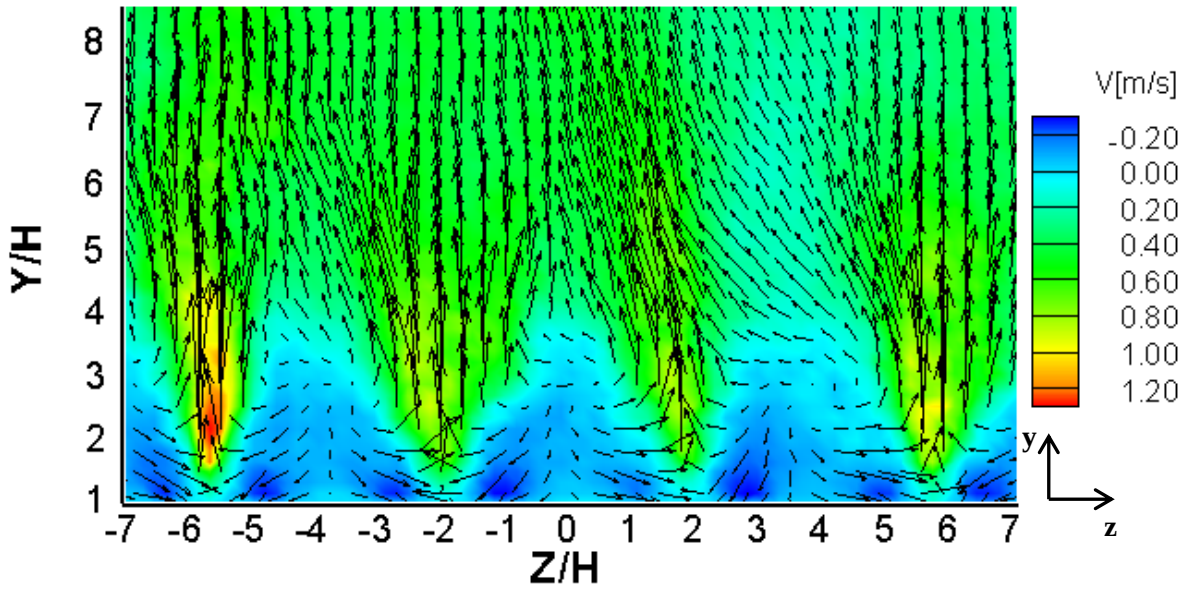

Figure 15. Induced Jet by the plasma actuator (PA3) at quiescent condition (6 KHz, 3.6 kV).

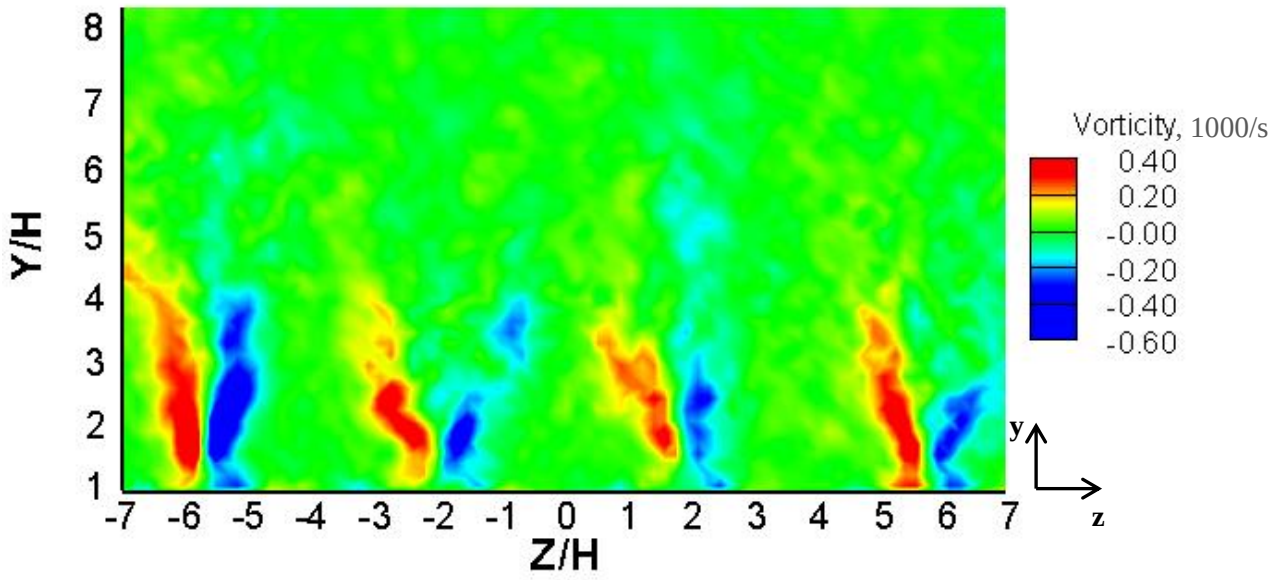

Figure 16. Vorticity contours generated by the plasma actuator (PA3) at quiescent condition (6 KHz, 3.6 kV).

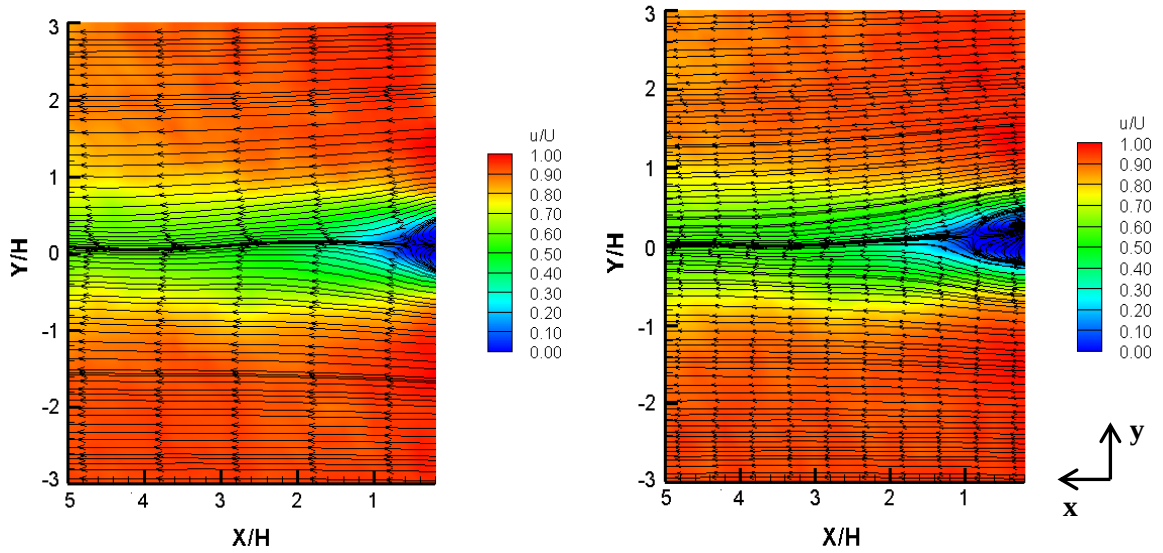

a) Plasma off b) plasma on (8 KHz, 4.2 kV)

Figure 17. Streamwise velocity component of blunt trailing edge flat plate with and without actuation of PA2 surface plasma actuator at free stream velocity of 7.5 ms^{-1} (flow from right to left).

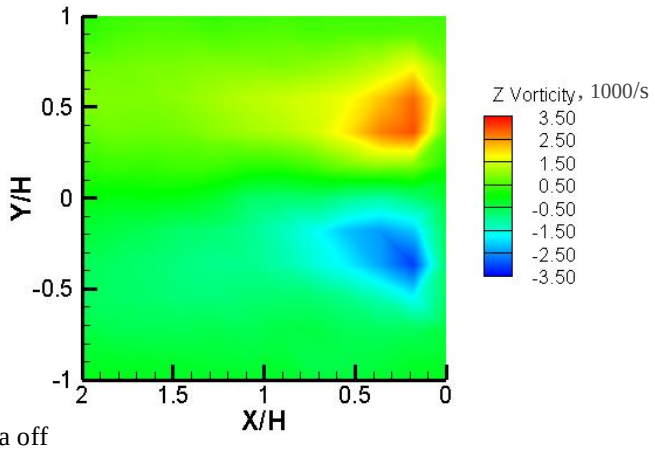

a) Plasma off

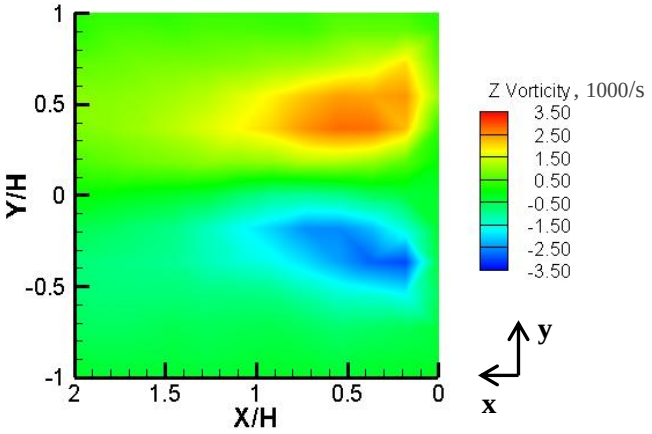

b) Plasma on (8 KHz, 4.2 kV)

Figure 18. Vorticity contour of blunt trailing edge flat plate with and without actuation of PA2 surface plasma actuator at free stream velocity of 7.5 ms^{-1} (flow is from right to left).

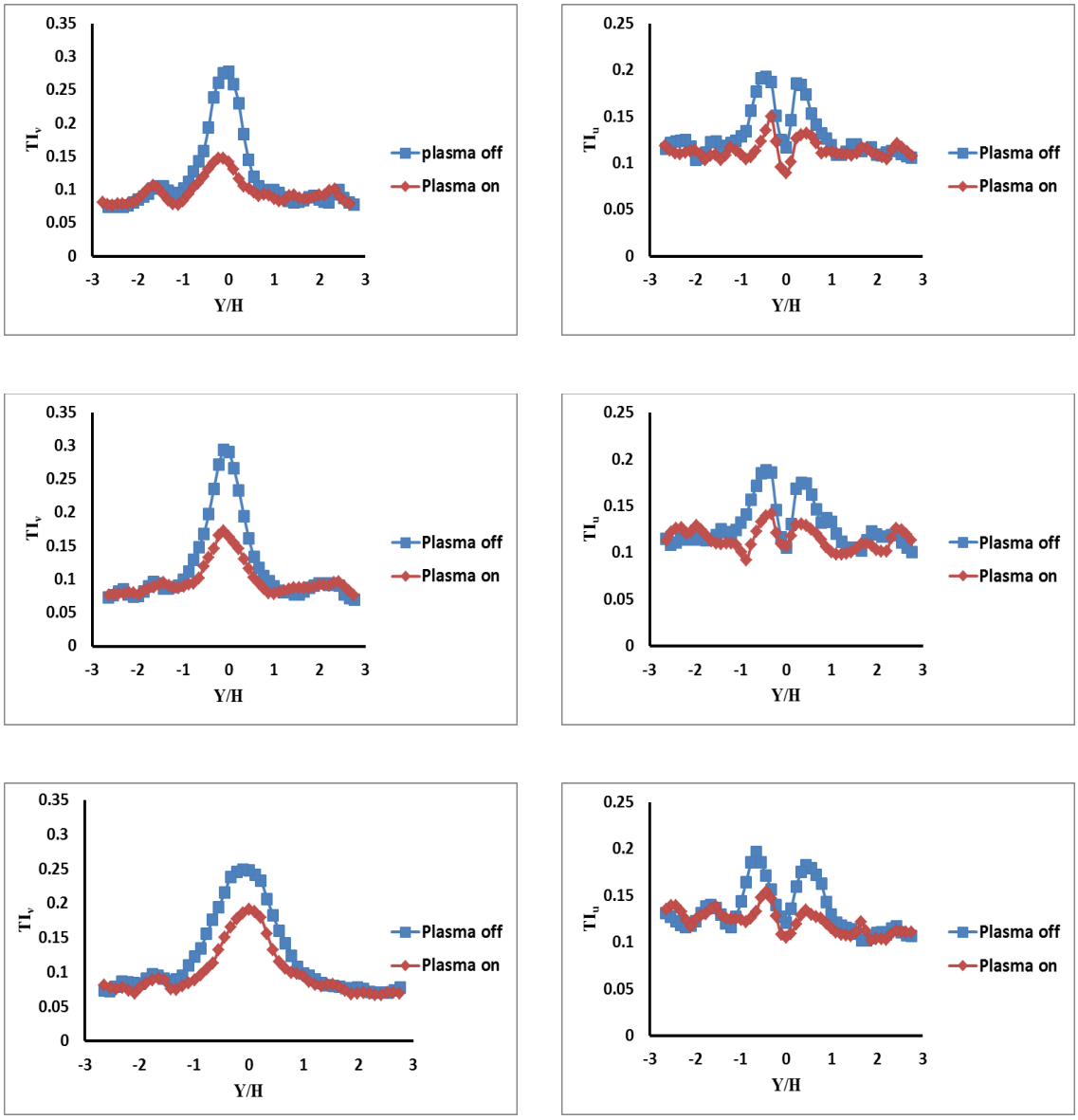

b) Vertical Turbulence intensity a) Streamwise Turbulence intensity

Figure 19. Wake turbulence intensity of blunt trailing edge flat plate with PA2 surface plasma actuator at free stream velocity of 7.5 ms^{-1} for downstream positions (3, 5, and 7 mm) top to bottom respectively.

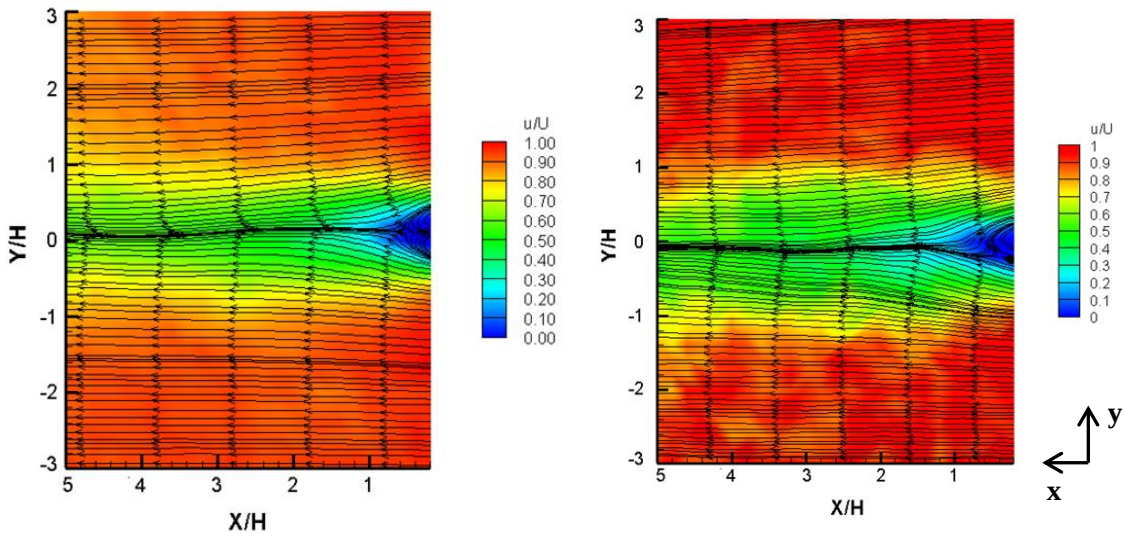

a) Plasma off b) plasma on (8 KHz, 4.2 kV)

Figure 20. Streamwise velocity component of blunt trailing edge flat plate with and without actuation of PA3 surface plasma actuator at free stream velocity of 7.5 ms^{-1} (flow from right to left).

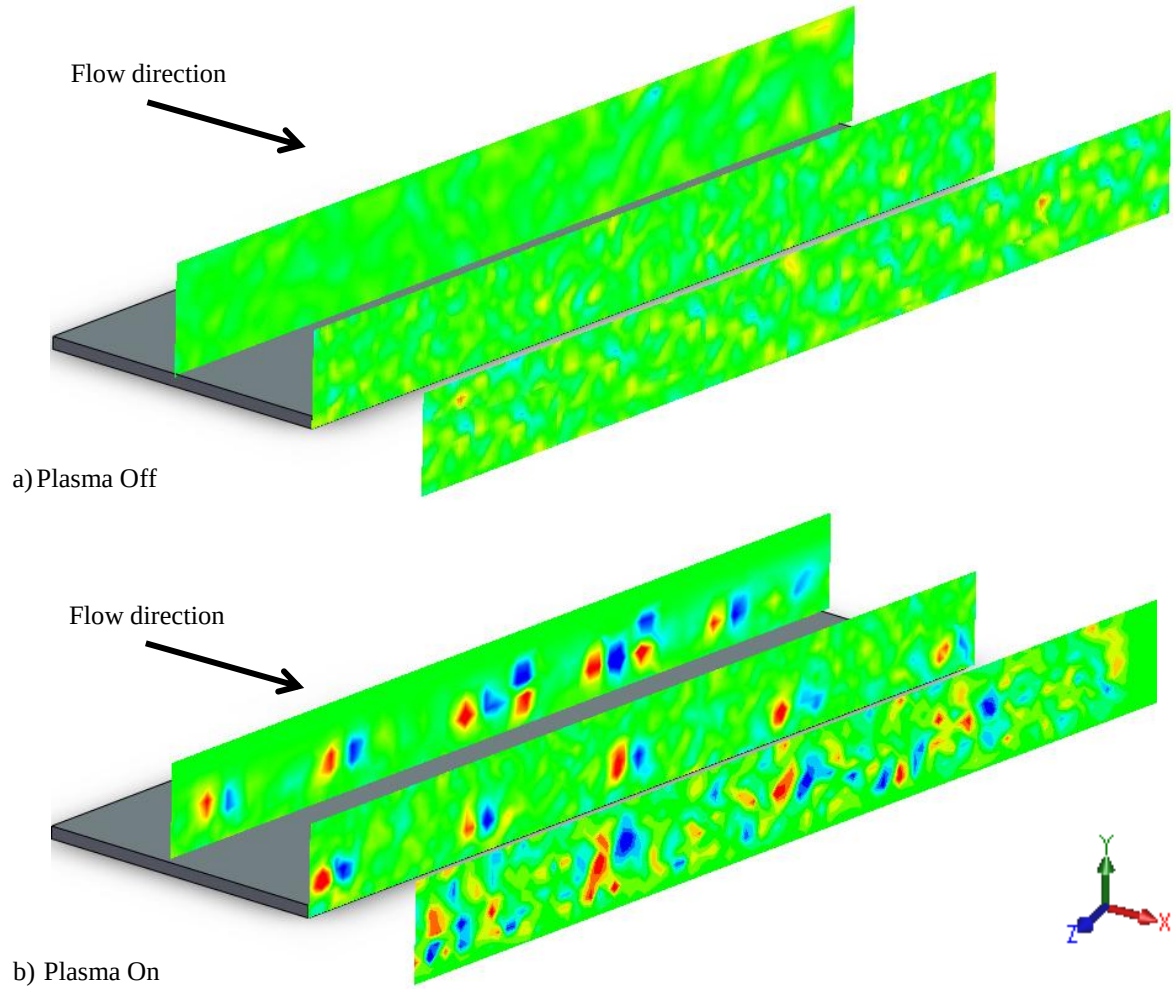

a) Plasma Off

b) Plasma On

Figure 21. Vorticity development contours of blunt trailing edge flat plate with the PA3 surface plasma actuator at free stream velocity of 7.5 ms^{-1}.

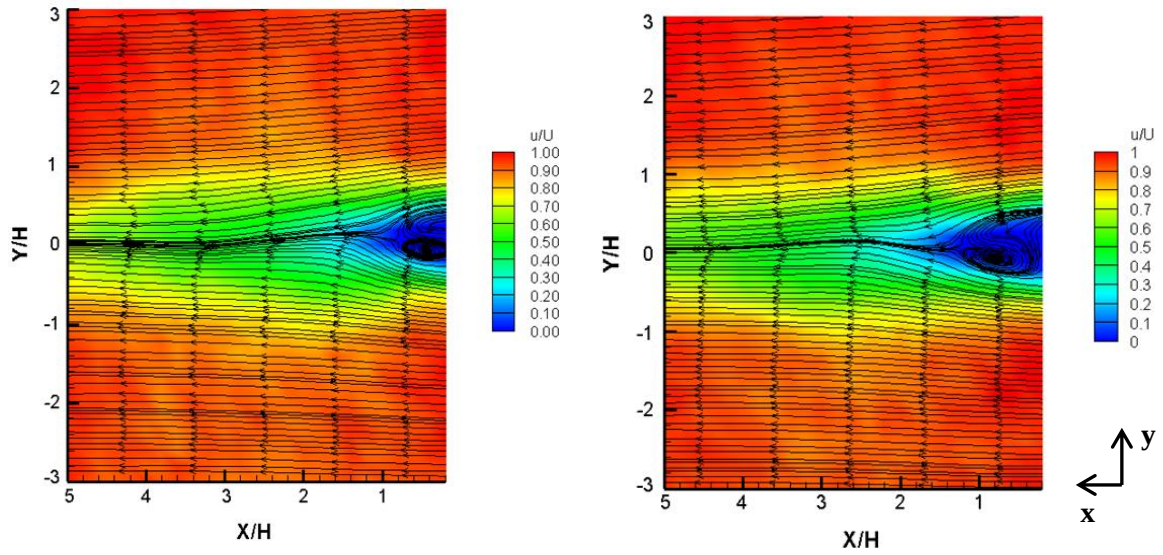

b) Plasma Off b) Plasma On (8 KHz, 4.2 kV)

Figure 22. Streamwise velocity component of rounded trailing edge flat plate with and without actuation of PA2 surface plasma actuator at free stream velocity of 7.5 ms^{-1} (flow from right to left).